Migration of mid-ocean-ridge volcanic segments

Hans Schouten*, Henry J. B. Dick* & Kim D. Klitgord†

* Woods Hole Oceanographic Institution, Woods Hole, Massachusetts 02543, USA
† US Geological Survey Woods Hole, Massachusetts 02543, USA

The propagation of small-offset volcanic spreading-centre segments along mid-ocean ridge crests may reflect absolute motion of the plate boundary relative to the underlying mesospheric frame. Such a relationship could be caused by a purely vertical flow of the mantle under spreading centres and would have value in constraining past plate motions from non-transform trends generated during along-ridge propagation and in linking the major-element variability of oceanic crust and upper mantle to the bulk composition and temperatures of mantle ascending under mid-ocean ridges.

MID-OCEAN ridges are offset by transform zones ranging in size from less than a kilometre to several hundred kilometres. Large-offset transform zones usually remain stationary relative to the plate boundary for many tens of millions of years, and divide the ridges into a series of relatively straight sections with lengths of tens to hundreds of kilometres. The sections are themselves segmented systematically by smaller offsets on a length scale of 30–80 km, which is related to spreading rate[1]. These small-scale volcanic segments have their origin in the asthenosphere under ridges where, at some depth beneath the axis, the mantle melt (magma) segregates from the partially molten mantle (the sub-axial asthensophere), concentrates at evenly spaced locations and drains quickly through cracks or diapirically to crustal magma chambers and associated volcanic spreading-centre segments[1–3].

Topographic lineaments

The volcanic segments have a pronounced topographic signature which is preserved in older crust as parallel topographic lineaments. Although these traces of past spreading-centre segmentation are sometimes developed parallel to flow-lines of relative plate motion[4], indicating that the volcanic segments did not propagate along the plate boundary, in other places these traces are oblique to flow-lines, forming broad V's about the spreading axis, indicating that the volcanic segments did propagate[5,6] (see Fig. 1*a* and *b*). These V-shaped non-transform traces on the segmentation scale should not be confused with the topographic and magnetic lineaments that mark propagating rifts[7,8]. These occur on a much larger length scale (typically hundreds of kilometres) and the non-transform pseudo-fault traces often indicate rift propagation in opposing directions. Such a geometry suggests a localized driving mechanism (such as the Galapagos and Cobb hotspots in the vicinity of the Galapagos and Juan de Fuca groups of propagating rifts).

The multiple non-transform traces associated with the volcanic segments, on the other hand, form a consistent set of features indicating propagation of a string of mid-ocean-ridge volcanic segments in one direction along the ridge crest. Such a geometry suggests a more regional driving mechanism (such as a sub-axial flow of the asthenosphere beneath the ridge[5]). In order to distinguish between these two classes of propagation phenomena we shall refer to the latter as migration.

In the slowly spreading North Atlantic, distant from known hotspots, sets of multiple non-transform lineaments have been mapped by detailed ridge-crest surveys at two places. At these locations, the chains of topographic highs and lows can be traced directly to the present-day segmentation of the ridge (Fig. 1*a* and *b*). The consistency of the non-transform trends indicates that in both cases the segments have been migrating along the spreading axis as a group. The non-transform traces of both Atlantic areas in Fig. 1 are symmetrical about an axis orthogonal to the spreading direction, but not about the oblique ridge crest. Calculated migration velocities that match these non-transform trends then depend on whether migration has occurred in a direction orthogonal to the spreading direction with symmetric spreading, or parallel to the oblique ridge crest with asymmetric spreading. Depending on the assumptions made, the migration velocity of the volcanic segments along the ridge is calculated at 49° N as 2.7 or 3.1 km Myr^{-1} respectively and at 26° N as 3.5 or 3.7 km Myr^{-1}.

On the fast-spreading East Pacific Rise (EPR), recent Seabeam investigations have revealed a fine-scale volcanic segmentation of the ridge axis[9–11]. The rather sparse off-axis survey data available show near-axis volcanic ridges or seamount chains with a significant non-transform direction[11,12] (Fig. 1*c* and *d*). Recent petrological studies of zero-age basalts dredged from the EPR axis suggest that mid-ocean-ridge volcanic segments are migrating southwards at overlapping spreading centres and saddle points near 12.9° N, 9.1° N, 8.6° N and 5.5° N (refs 13, 14). Magnetic studies of overlapping spreading centres near 11.7° N and 9.1° N also suggest a southward migration[15,16]. The petrological and magnetic conclusions are consistent with the direction of migration indicated by the off-axis non-transform trends. This section of the EPR is distant from any known hotspots. The Pacific non-transform trends in Fig. 1 indicate southward migration at similar velocities though separated by more than 500 km.

The seamount chains in Fig. 1*c* and *d* appear to occur only on one side of the spreading axis, and are thus different from the symmetrical parallel traces in the Atlantic. Furthermore, the near-axis chains are generally shallower than the rise axis, suggesting voluminous off-axis volcanic activity. Lonsdale[11] attributed the chain near 5.5° N to southward migration of the dextral overlapping spreading centre at 5.5° N. The chain at 10° N was related by Crane[3] to an axial high at 9.83° N, but might equally be associated with a small dextral ridge offset nearby (see Fig. 1*c*). The one-sided distribution of the two Pacific non-transform traces might thus be related to southward migration of dextral offsets between volcanic segments and analogous to the one-sided failed rifts in the propagating rift geometry[17] (see also Fig. 2*a*). The shallow depth of these near-axis seamount chains then suggests that young failed rift zones would be a locus of significant off-axis volcanic activity.

Flow of asthenosphere

If the origin of such observed non-transform traces lies in a sub-axial asthenosphere flow[5], it is now necessary to ask whether that flow has any regularity. The orientation of the non-transform traces of Fig. 1 relates qualitatively to the absolute plate motions deduced from hotspot traces, shown schematically in Fig. 2. This concept was tested using the absolute plate motion model AM1-2 of Minster and Jordan[18]. We find that a southward sub-axial asthenosphere flow of 28 km Myr^{-1}, estimated from the Pacific non-transform traces of Fig. 1, correlates with the

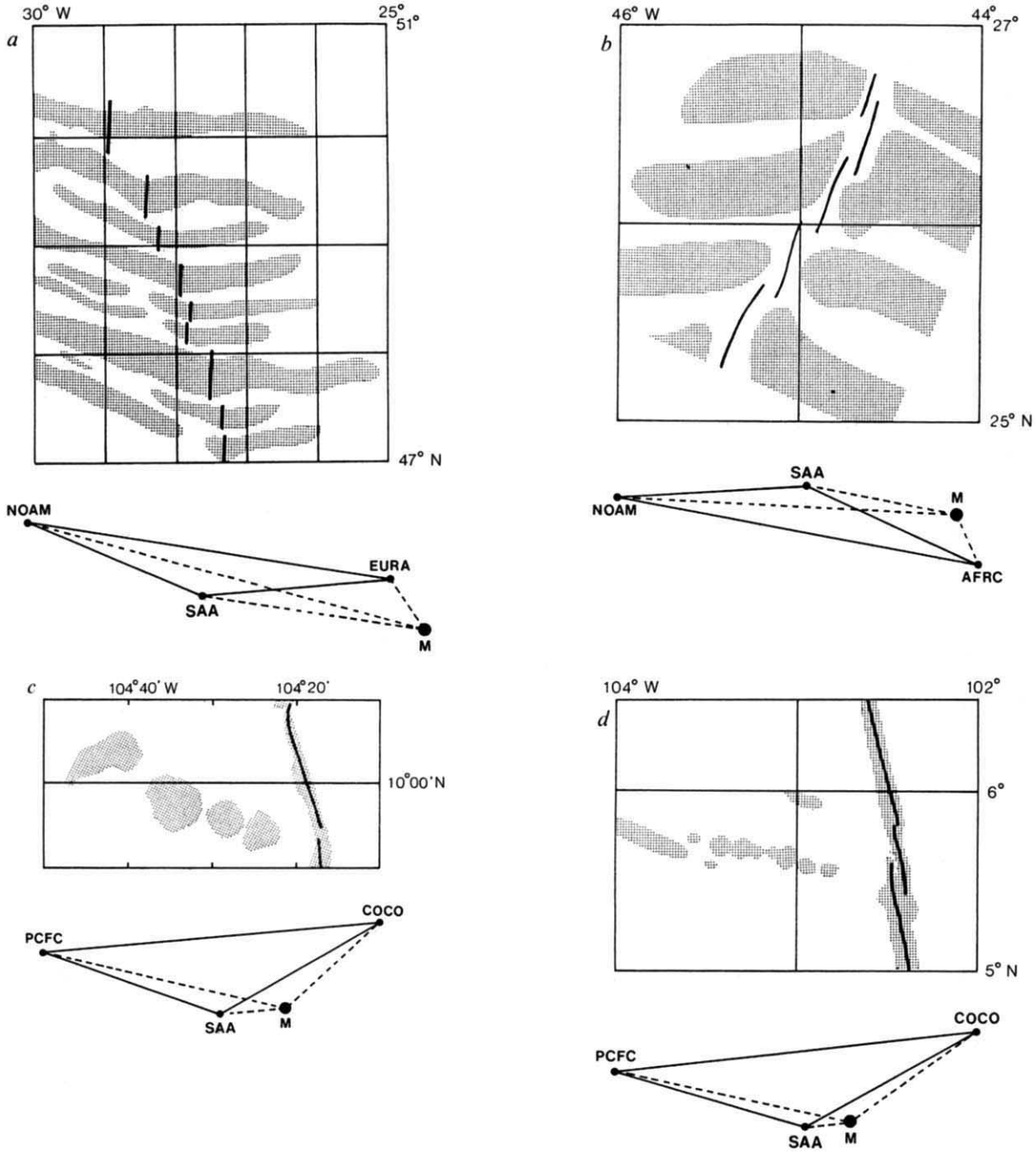

Fig. 1 Non-transform patterns of ridge crest indicating migration of volcanic segments in the Atlantic and eastern Pacific. *a*, North Atlantic plate boundary (NOAM–EURA). Stippled areas show interpreted trends of topographic belts which clearly form broad V's about the spreading axis (after ref. 5). The belts can be traced directly to the present-day segmentation of the active ridge (short heavy lines, modified after ref. 5). The oblique angles of the recent (<5 Myr) trends indicate southward migration velocities of ~3 km Myr^{-1}. *b*, Central Atlantic plate boundary (NOAM–AFRC). Stippled areas show recent (<5 Myr) topographic highs separated by pronounced topographic lows which can be traced to small offsets between the active spreading centre segments (modified after ref. 6). The angles of these trends indicate northward migration velocities of ~3.5 km Myr^{-1}. *c*, East Pacific plate boundary near 10° N (PCFC–COCO). Stippled areas show water depths shallower than 2,600 m, the heavy lines show the spreading-centre segments (after ref. 12). The near-axis seamount chain can be explained alternatively as the one-sided trace of an axial high at 9.83° N migrating southward[3] or off-axis volcanic activity marking a young failed rift zone caused by southward migration at ~28 km Myr^{-1} of the small dextral offset between segments at 9.9° N. *d*, East Pacific plate boundary near 5.5° N (PCFC–COCO). Stippled areas show water depths shallower than 3,000 m and the heavy lines the active spreading centre segments (after ref. 11). The major non-transform seamount chain on the young Pacific plate can be related to the dextral overlapping spreading centre at 5.5° N and its migration southward at ~25 km Myr^{-1} (ref. 11). A minor topographic lineament to the north of this chain can similarly be related to a small dextral offset between segments at 5.85° N.

The non-transform trends in (*c*) and (*d*) are separated by more than 500 km but yield similar migration velocities in the same direction suggesting a regional sub-axial flow of asthenosphere beneath the boundary between the Pacific and the Cocos plate. The velocity-space diagrams (explained in Fig. 2) show the non-transform trends (SAA to plate) predicted for the four ridge locations from Pacific absolute plate motion vectors[18] (*c* and *d*) and from adjusted Atlantic vectors (*a* and *b*) which are consistent with the observed non-transform trends and with the absolute plate motion model AM1-2 within its limits of error as shown in Table 1. This analysis indicates that a sub-axial asthenosphere flow, which would cause volcanic segments to migrate, could be driven by the absolute motion of the plates.

Table 1 Atlantic absolute motion vectors

Plate	θ ° N	σ_θ deg.	ϕ ° E	σ_ϕ deg.	ω deg. Myr^{-1}	σ_ω deg. Myr^{-1}
AFRC*	18.76	33.93	−21.76	42.20	0.139	0.055
EURA*	0.70	124.35	−23.19	146.67	0.038	0.057
NOAM*	−58.31	16.21	−40.67	39.62	0.247	0.080
AFRC†	30.00	—	−34.00	—	0.191	—
EURA†	33.78	—	−49.80	—	0.092	—
NOAM†	−42.86	—	−48.64	—	0.243	—

* Absolute motion model AM1-2 of Minster and Jordan[18].

† Data from this study. These vectors obey the relative motion model RM2 of Minster and Jordan[18] and are used to construct the velocity space diagrams for Fig. 2*a* and *b*.

ridge-parallel component of apparent motion of the mesosphere relative to a symmetrically spreading East Pacific Rise as shown by the velocity diagrams for the two Pacific locations in Fig. 1.

The AM1-2 is not well constrained for the North Atlantic plates. The deduced migration rates of 3 km Myr^{-1} southward at 49° N and 3.5 km Myr^{-1} northwards at 26° N are, however, consistent with the Atlantic absolute motion vectors within their limits of error. We have used the non-transform trends, the relative motion model RM2 (ref. 18) and the assumption of symmetric spreading to recalculate present-day absolute motion vectors of the North American, Eurasian and African plates, which are given in Table 1, together with the AM1-2 vectors and their estimated uncertainties. These adjusted vectors were used to construct the velocity diagrams for the two Atlantic locations in Fig. 1.

From this analysis we propose that the sub-axial asthenosphere flow, which causes volcanic segments to migrate along ridge axes, is driven by the absolute motion of the plates. The migration equals the axis-parallel component of motion of the hot-spot frame relative to the spreading plates at their boundary (see Fig. 2). We now examine the consequences of this postulate.

Upwelling of mantle

First, a correlation between the migration of volcanic segments along the ridge and absolute plate motions implies that the volcanic segments are closely linked to the mesosphere and that, similar to the mesosphere, the framework from within which they originate must have horizontal absolute motions much slower than the motions of the plates. If the volcanic segments represent persistent melting anomalies within the upper mantle under ridges as argued by Whitehead *et al.*[2], then this part of the upper mantle must be below the zone of shearing that, in a broad sense, must separate the mesosphere and its motion from those of the lithospheric plates. Since the depth of segregation of melt from the shallow mantle may be no more than a few tens of kilometres below ocean spreading centres (see ref. 2), this in turn implies that, directly under ridges, the mesospheric frame exerts a strong influence to within a short distance of the surface of the Earth. On this basis, the mantle which rises toward mid-ocean ridges would rise essentially vertically in the mesospheric framework to a very shallow level and release its melt before it enters the shear zone between mantle and the lithospheric plates beneath the ridge. The absolute motion vector of the sub-axial asthenosphere (M-SAA in Fig. 2*c*) then represents the progression through the ascending mantle of the locus of highest melt production or, the locus of fastest and shallowest mantle upwelling between the separating plates.

Next, consider a kinematic model (shown in the ridge-fixed frame in Fig. 3) in which the mantle rises vertically under mid-ocean ridges that move laterally over the mantle. Decoupling between vertical upwelling of mantle and horizontal plate motions is assumed for simplicity to take place in an infinitesimally thin shear zone at the base of the lithosphere.

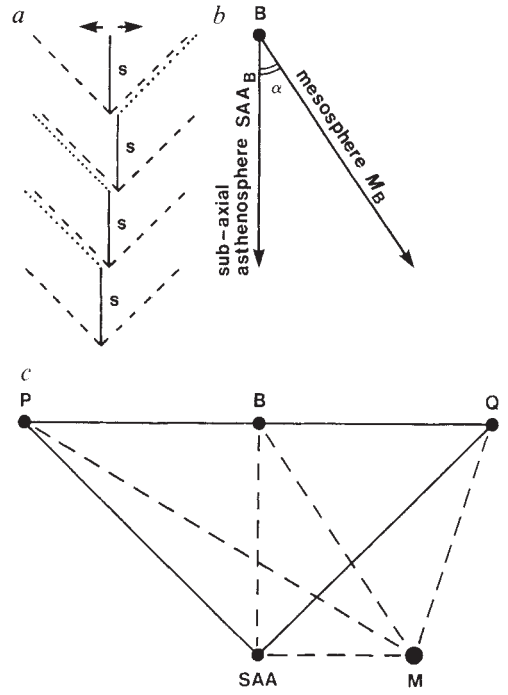

Fig. 2 *a*, Small-offset volcanic spreading-centre segments (s) propagate at a uniform velocity in the same direction along the boundary between two separating lithospheric plates, leaving multiple and parallel non-transform traces in older crust away from this boundary. The dashed lines represent the pseudo-faults[7], the symmetric traces of transition zones between consecutive volcanic segments where topographic lows can be expected. The one-sided dotted lines represent the failed rift zones[17], the deactivated tail ends of the active spreading-centre segments left on one plate or the other by propagation of the next volcanic segment. The young failed rift zones could be a locus of off-axis volcanic activity forming one-sided non-transform volcanic ridges or seamount chains. The angle of the non-transform trends is a measure of the propagation velocity. *b*, The propagation of a string of small-offset volcanic spreading-centre segments (here referred to as migration) can be explained by a flow of the sub-axial asthenosphere beneath the ridge which is directly related to the motion of the plate boundary in the fixed-hotspot mesospheric reference frame. Motions of the sub-axial asthenosphere (SAA_B) and the mesospheric frame (M_B) are referenced to the plate boundary (B). $SAA_B = M_B \cos \alpha$. *c*, The geometry in velocity space of the postulated motion of the sub-axial asthenosphere (SAA) relative to the two separating plates (P and Q), the plate boundary (B, assuming symmetric seafloor spreading), and the fixed-hotspot mesospheric reference frame (M). The heavy line connecting P and Q denotes the relative plate motion, the heavy lines connecting SAA with P and Q denote the postulated non-transform trends. The dashed lines denote the 'sub-axial asthenosphere flow' (B to SAA), and the absolute motions of the various reference frames.

Conservation of mass requires that the vertical flow of mantle (V_z) in the wake of the separating and growing lithospheric plates is then proportional to the slope of the base of the lithosphere (θ) and to the normal-to-axis velocity (V_p) of each plate relative to the 'fixed' mantle or, $V_z = V_p \tan \theta$ (ref. 19). The fastest upwelling of shallow mantle and consequent highest melt production by decompression occurs beneath the ridge and thus moves relative to the mesosphere with the normal-to-axis component of absolute plate boundary motion (see also Fig. 2).

The ratio between total spreading rate and normal-to-axis velocity of the spreading axis over the mantle (which we define as the mantle consumption ratio) is then a measure of the total mantle upwelling required to balance the growth of the spreading lithospheric plates. This ratio scales the flow field under both spreading plates and scales the depth to which spreading

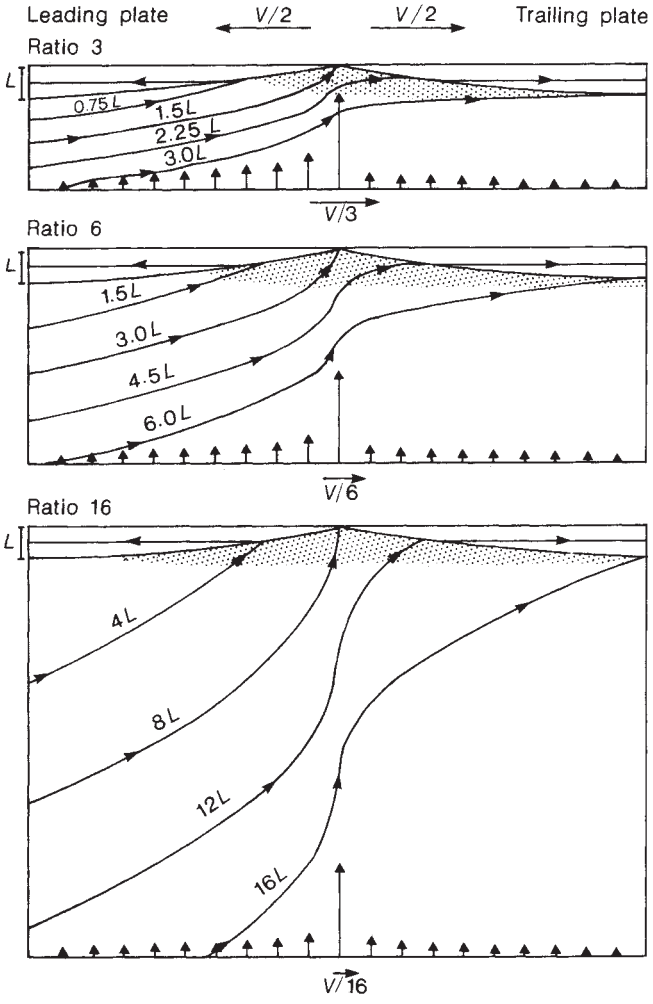

Fig. 3 Kinematic model of whole-mantle upwelling under symmetrically spreading ridges moving laterally over the mantle (shown in the ridge-fixed frame). This model assumes purely vertical flow of mantle material (in the absolute motion reference frame) and a decoupling between vertical mantle upwelling and horizontal plate motion at the base of the lithospheric plates. Vertical mantle flow (vertical arrows) is then proportional to the slope of the base of the lithosphere and the normal-to-axis velocity of each plate relative to the 'fixed' mantle (after ref. 19). Horizontal arrows beneath each diagram give the apparent horizontal motion of the mantle reference frame relative to the ridge. The stream lines, which show how the underlying mantle would appear to move to an observer on the ridge, predict significant asymmetries in paths and melt histories of mantle material that underplates the leading or the trailing lithospheric plate, and a path and melt history of mantle material that forms the upper mantle under oceanic crust that is dependent on the mantle consumption ratio (total spreading rate divided by the normal-to-axis velocity of a symmetrically spreading ridge relative to the mantle). Initial depths of mantle material now upwelling to balance the growth of the spreading lithospheric plates, are given in thickness of older lithosphere (L, assumed to be constant outside the diagrams). Diagrams for mantle consumption ratios 3 and 16 predict the shallower upwelling under the American-Antarctic Ridge and South-west Indian Ridge, and deeper upwelling under the southern Mid-Atlantic Ridge near the Bouvet Triple Junction, respectively. Stippled areas give schematically the melting region for a mantle of uniform composition, determined by the particular geotherm chosen as the initial boundary condition at the start of adiabatic mantle upwelling on the left of the diagrams. The lowest degree of mantle melting occurs near the base of the melting region (that is, the mantle solidus), the highest degree occurs directly beneath the thin lithosphere at the spreading axis and is related to initial depth or, mantle consumption ratio.

plates must ideally 'consume' underlying mantle (see Fig. 3). For higher consumption ratios, deeper mantle will be added to the lithosphere; for a ratio of x, the spreading plates would ultimately have consumed upper mantle equal to roughly x thicknesses of older lithosphere (L in Fig. 3 which is assumed to be constant outside the diagrams). In the case of a thicker shear zone at the base of older lithosphere, mass balance will require a greater mantle upwelling than with the infinitesimal shear zone in Fig. 3. Typically, the present-day ratios calculated from the AM1-2 model vary from ~2 to ~7 or higher, and they may vary considerably along any boundary.

Degree of mantle melting

The degree of partial melting of the mantle emplaced to the base of the crust at spreading centres is largely determined by its total depth of upwelling. For a mantle of homogeneous bulk composition and no contaminating fluids leaking into the shallow mantle from below, the degree of melting of the shallowest mantle under spreading centres then becomes a function of its initial depth and the initial geotherm (that is, the depth and geotherm before significant mantle upwelling due to an approaching mid-ocean-ridge system). Because this initial geothermal gradient was probably more conductive than adiabatic in the thermal boundary layer, in the shallower mantle under the plates, mantle ascending adiabatically from a shallower initial depth will be less molten than mantle ascending from greater initial depths (see ref. 20).

Some of the deepest mantle upwelling (and highest degree of mantle melting) is predicted for the southern Mid-Atlantic Ridge (SMAR) between South America and Africa near the Bouvet Triple Junction where the ridge has apparently remained nearly fixed in the absolute motion frame since the Mesozoic break-up of the continent of southern Gondwana (see ref. 21). In contrast, shallower upwelling (and lower degree of mantle melting) is predicted for the American-Antarctic Ridge (AAR) and the south-west Indian Ridge (SWIR) immediately to the west and east of the triple junction where the trailing plate (Antarctica) has remained relatively stationary. (A stationary ridge implies a very high mantle consumption ratio, a stationary trailing plate implies a ratio of 2.) The AM1-2 model yields present-day mantle consumption ratios of 16.4 for the SMAR (for the equatorial MAR this ratio is 3.5) and 2.7 for both AAR and SWIR near the triple junction.

Basaltic lavas dredged along these ridges exhibit systematic differences in major-element composition (Fig. 4) related to differences in degree of melting of the shallow mantle under the ridges with which the melt equilibrates before segregation and eruption[22]. Figure 4 shows the fields for the Ca/(Ca+Na) and Mg/(Mg+Fe) ratios of 574 basaltic glasses from these ridges, with glasses from the SWIR separated into those dredged far from and near to the Bouvet mantle plume. As can be seen, the glasses from the Bouvet mantle plume region, and those from the southern end of the MAR plot are along approximately the same linear trend across the diagram. In contrast the glasses from the SWIR, far from the Bouvet mantle plume, and those from the AAR plot are along a similar parallel linear trend lower in the diagram.

This plot is particularly useful in that it uses simple binary oxide ratios and effectively separates liquidus trends for different primary magmas. In addition, the effects of fractional crystallization are easily distinguished from those due to varying degrees of melting (or initial source composition). As shown in the inset, variable degrees of melting of the mantle produces a relatively small variation in Mg/(Mg+Fe) of the partial melt, but a large variation in Ca/(Ca+Na). In contrast, fractional crystallization of olivine and plagioclase from a melt produces large variations in both ratios in a sense opposite to that for increasing degrees of mantle melting.

The systematic offset in Fig. 4 between the fields for the AAR and SWIR, and the field for the SMAR reflect the similar low

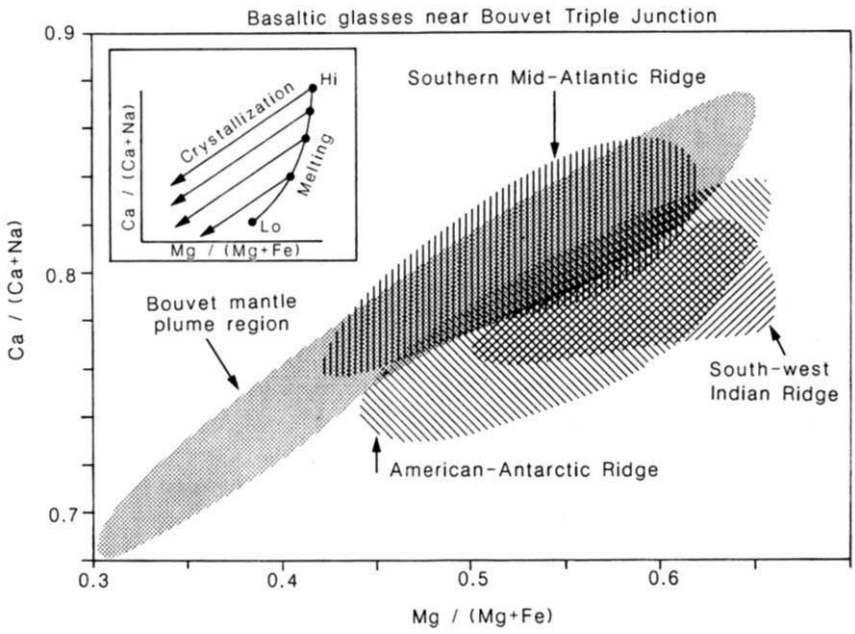

Fig. 4 Composition of basaltic glasses dredged near the Bouvet Triple Junction of the South American, African, and Antarctic plates. As shown by the inset cartoon, increasing degree of mantle melting produces melts with slowly increasing Mg/(Mg+Fe) and rapidly increasing Ca/(Ca+Na). Subsequent fractionation of melts representing different degrees of melting during crystallization and cooling, will produce systematically offset trends of decreasing Mg/(Mg+Fe) and Ca/(Ca+Na). The basalts dredged from the American-Antarctic Ridge (2°-18° W) and South-west Indian Ridge away from the Bouvet mantle plume (5°-25° E), both plot along lower trends in the diagram, reflecting lower degrees of melting of the parent mantle, than basalts dredged from the southern Mid-Atlantic Ridge (51°-55° S). The basalts from the southern Mid-Atlantic Ridge plot along virtually the same trend as basalts from the Bouvet mantle plume region (1°-5° E), reflecting a high degree of melting and deep mantle upwelling for both regions. The isotopic composition of basalts from these two regions is significantly different, precluding an origin for the southern Mid-Atlantic Ridge basalts related to the Bouvet plume (A. Le Roex, personal communication). The plume-like deep upwelling suggested by the high degrees of melting under the southern Mid-Atlantic Ridge and the shallower upwelling predicted from lower degrees of melting of the mantle under the other two ridges are explained with the geometry of absolute plate motions particular to this area and the existence of a significant thermal boundary layer beneath the lithosphere of southern Gondwana before the Mesozoic break-up of that continent.

degrees of melting of the mantle beneath the AAR and SWIR, and the higher degree of melting beneath the SMAR, as was predicted from our model. Furthermore, the high Ca/(Ca+Na) ratios of basalts dredged from the Bouvet mantle plume region and from the SMAR are indistinguishable, confirming the plume-like deep mantle upwelling and consequent highest degrees of mantle melting beneath the SMAR that this kinematic model (Fig. 3) would predict. The same high Ca/(Ca+Na) ratios against Mg/(Mg+Fe) also characterize the zero-age basalts dredged from the EPR (J. Natland, personal communication) suggesting that their mantle parent also rose from great initial depths. This is consistent with the low estimates of net absolute motion of this plate boundary over the past 100 Myr (refs 23, 24) for which our model independently predicts deep mantle upwelling in the East Pacific region.

Markers of absolute plate motion

A final consequence of our postulate is that non-transform traces produced by migration of volcanic ridge segments provide estimates of absolute plate motion, present and past, independent of the hotspot traces. Such estimates can be important in reconstructing motions of plates with ill-defined hotspot traces.

Considering the affinity to the mesospheric frame of the migration of volcanic segments along Pacific and Atlantic mid-ocean ridges, a predominantly vertical mantle flow beneath these ridges seems likely. This is supported by the correlation between the degree of melting of the shallow mantle under ridges and net absolute plate boundary motion. If our observations and interpretations of migration of mid-ocean ridge volcanic segments can be applied to present and past ridges on a global scale, it could provide a new and compelling argument for whole-mantle convection (see ref. 25). A comprehensive examination of the major-element variability of zero-age basalts could then provide important constraints on the bulk composition and temperatures of mantle upwelling under mid-ocean ridges.

Many of the ideas presented here have been nurtured by the weekly WHOI Geodynamics seminars sponsored by the Center for Analysis of Marine Systems (CAMS) of the Woods Hole Oceanographic Institution with funds from the Exxon Education Foundation. We thank D. Epp, R. C. Kerr, J. Phipps Morgan, J. Natland, W. Normark, A. Trehu, J. A. Whitehead and especially J. R. Cann for constructive criticism. This work was supported by the Office of Naval Research and the NSF. Pam Foster and Maureen Carragher processed the manuscript.

Received 29 December 1986; accepted 11 February 1987.

1. Schouten, H., Klitgord, K. D. & Whitehead, J. A. *Nature* **317**, 225-229 (1985).
2. Whitehead, J. A., Dick, H. J. B. & Schouten, H. *Nature* **312**, 146-148 (1984).
3. Crane, K. *Earth planet. Sci. Lett.* **72**, 405-414 (1985).
4. Schouten, H. & Klitgord, K. D. *Earth planet. Sci. Lett.* **59**, 255-266 (1982).
5. Johnson, G. L. & Vogt, P. R. *Geol. Soc. Am. Bull.* **84**, 3443-3462 (1973).
6. Rona, P. A., Harbison, R. N., Bassinger, B. G., Scott, R. B. & Nalwalk, A. J. *Geol. Soc. Am. Bull.* **87**, 661-674 (1976).
7. Hey, R. & Vogt, P. *Tectonophysics* **37**, 41-52 (1977).
8. Hey, R. N. & Wilson, D. S. *Earth planet. Sci. Lett.* **58**, 167-188 (1982).
9. Macdonald, K. C. & Fox, P. J. *Nature* **302**, 55-58 (1983).
10. Macdonald, K. C., Sempere, J.-C. & Fox, P. J. *J. geophys. Res.* **89**, 6,049-6,069 (1984).
11. Lonsdale, P. *Geol. Soc. Am. Bull.* **96**, 313-327 (1985).
12. Fornari, D. J., Ryan, W. B. F. & Fox, P. J. *J. geophys. Res.* **89**, 11069-11083 (1984).
13. Hekinian, R. *et al. Mar. geophys. Res.* **7**, 359-377 (1985).
14. Langmuir, C. H., Bender, J. F. & Batiza, R. *Nature* **322**, 422-429 (1986).
15. Sempere, J.-C., Macdonald, K. C. & Miller, S. P. *Geophys. J. R. astr. Soc.* **79**, 799-811 (1984).
16. Sempere, J.-C. & Macdonald, K. C. *Eos* **67**, 1227 (1986).
17. Hey, R., Duennebier, K. & Morgan, W. J. *J. geophys. Res.* **85**, 3647-3658 (1980).
18. Minster, J. B. & Jordan, T. H. *J. geophys. Res.* **83**, 5331-5354 (1978).
19. Davis, E. E. & Karsten, J. L. *Earth planet Sci. Lett.* **79**, 385-396 (1986).
20. McKenzie, D. *J. geophys. Res.* **25**, 713-765 (1984).
21. Morgan, W. J. *Tectonophysics* **94**, 123-139 (1983).
22. Dick, H. J. B., Fisher, R. L. & Bryan, W. B. *Earth planet. Sci. Lett.* **69**, 88-106 (1984).
23. Jurdy, D. M. & Gordon, R. G. *J. geophys. Res.* **89**, 9927-9936 (1984).
24. Schult, F. R. & Gordon, R. G. *J. geophys. Res.* **89**, 1,789-1,800 (1984).
25. Loper, D. E. *J. geophys. Res.* **90**, 1809-1836 (1985).